10 Applied Science

10-1 The Chemistry, Band Offsets and Annealing Behaviors of HfO_2 Thin Films for ULSI Gate Dielectrics

High dielectric constant (high-*k*) materials have been extensively investigated as alternatives to SiO_2 since the downscaling of complementary metal-oxide semiconductor (CMOS) field effect transistor (FET) dimensions results in increasing levels of leakage current. In particular, hafnium dioxide (HfO_2) has a high potential for next-generation device applications such as ultra large scale integration (ULSI) due to its considerably large energy-band gap, high-*k* and compatibility with conventional CMOS processes thanks to its thermal stability. However, there are some problems to be solved such as the suppression of interfacial silicate layer formation and the control of band offsets and thermal stability during activation processes. To fabricate high-quality gate insulators with well-controlled interlayers, the interfacial chemistry, band offsets and chemical state change due to the subsequent annealing must be investigated systematically. Here, we report the development of a substrate subtraction method for precisely determining valence band offsets using photoelectron spectroscopy (PES) [1], and a new method for determining conduction band offsets using X-ray absorption spectroscopy (XAS) [2]. Furthermore, the combined technique of *in situ* annealing and high-resolution PES has revealed the thermal stability of HfO_2/Hf-silicate/Si stacks [3].

The experiments were carried out at BL-2C, which is equipped with a high-resolution photoelectron analyzer (GAMMADATA-SCIENTA SES100). $HfO_2/Hf_{1-x}Si_xO_2/Si$ samples were prepared using a magnetron sputtering method. The transmission electron microscopy (TEM) image shown in Fig. 1 reveals that the film consists of 1.6 nm of HfO_2 and 2.8 nm of $Hf_{1-x}Si_xO_2$. After confirming that subtraction of the valence band photoelectron spectrum of H-terminated Si from that of SiO_2/Si results in the appropriate deduction of 4.4 eV for the SiO_2/Si band offset, we have applied this method to the $HfO_2/Hf_{1-x}Si_xO_2/Si$ system, revealing valence band offsets of ΔE_v^1 = 3.8 eV for $Hf_{1-x}Si_xO_2$/Si and ΔE_v^2 = 3.0 eV for HfO_2/Si, as shown in Fig. 2(a). Following these measurements, we attempted to apply a new method to precisely determine the band gap of the double layer structure by using XAS. After confirming the validity of this method using the SiO_2/Si sample with 8.9 eV of band gap, we applied this method to the $HfO_2/Hf_{1-x}Si_xO_2/Si$ system, revealing band gaps of ΔE_g^1 = 8.6 eV for $Hf_{1-x}Si_xO_2$/Si and ΔE_g^2 = 5.1 eV for HfO_2/Si. Figs. 2(b) and 2(c) show the XAS spectra for $HfO_2/Hf_{1-x}Si_xO_2/Si$ and the determined band offsets. Knowledge of the band offsets is very important for designing CMOS-FET gate stacks.

Next, we have investigated the changes in chemical states of the $HfO_2/Hf_{1-x}Si_xO_2/Si$ system due to in vacuum annealing. Fig. 3 shows Hf 4*f* core-level spectra of as-grown and subsequently annealed samples at 800, 900, and 1000°C. In the case of annealing at 900°C a small peak due to the metallic Hf and Hf-silicide component can be seen for Sample A ($HfO_2/Hf_{1-x}Si_xO_2/Si$ without Hf predeposition), but this structure is not observed for Sample B ($HfO_2/Hf_{1-x}Si_xO_2/Si$ with Hf predeposition). This shows that Hf-metal predeposition (Sample B) can suppress the formation of Hf-silicide and segregation of the Hf metal at the interface even after 900°C annealing, probably playing a significant role in suppressing the gate leakage

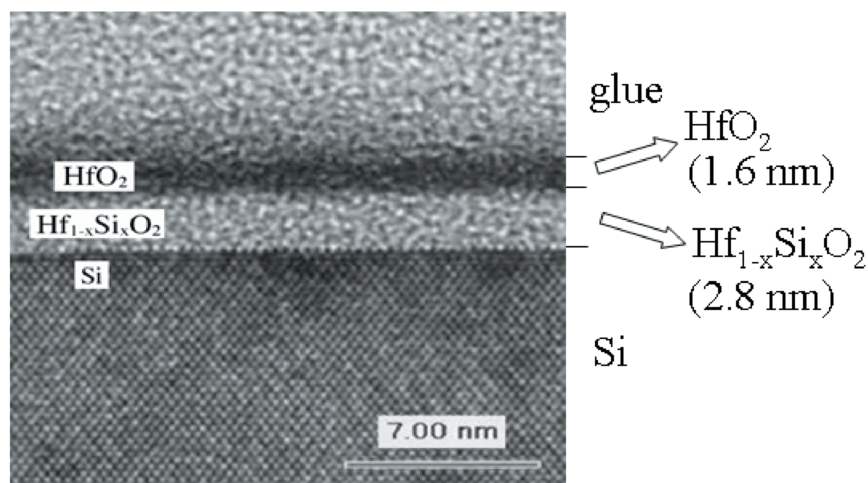

Figure 1
Cross-sectional TEM image of $HfO_2/Hf_{1-x}Si_xO_2/Si$.

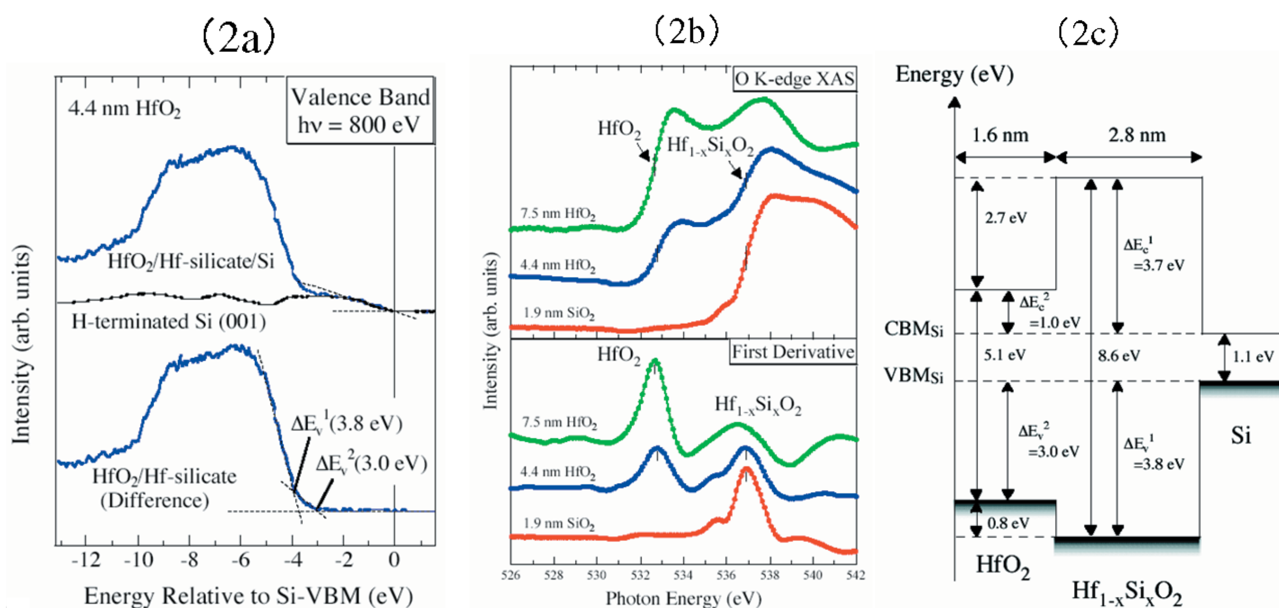

Figure 2

Valence band photoelectron spectra (a), and X-ray absorption spectra (b) for $HfO_2/Hf_{1-x}Si_xO_2/Si$, and the determined energy band diagram (c). VBM_{Si} and CBM_{Si} represent the valence band maximum and conduction band minimum of silicon.

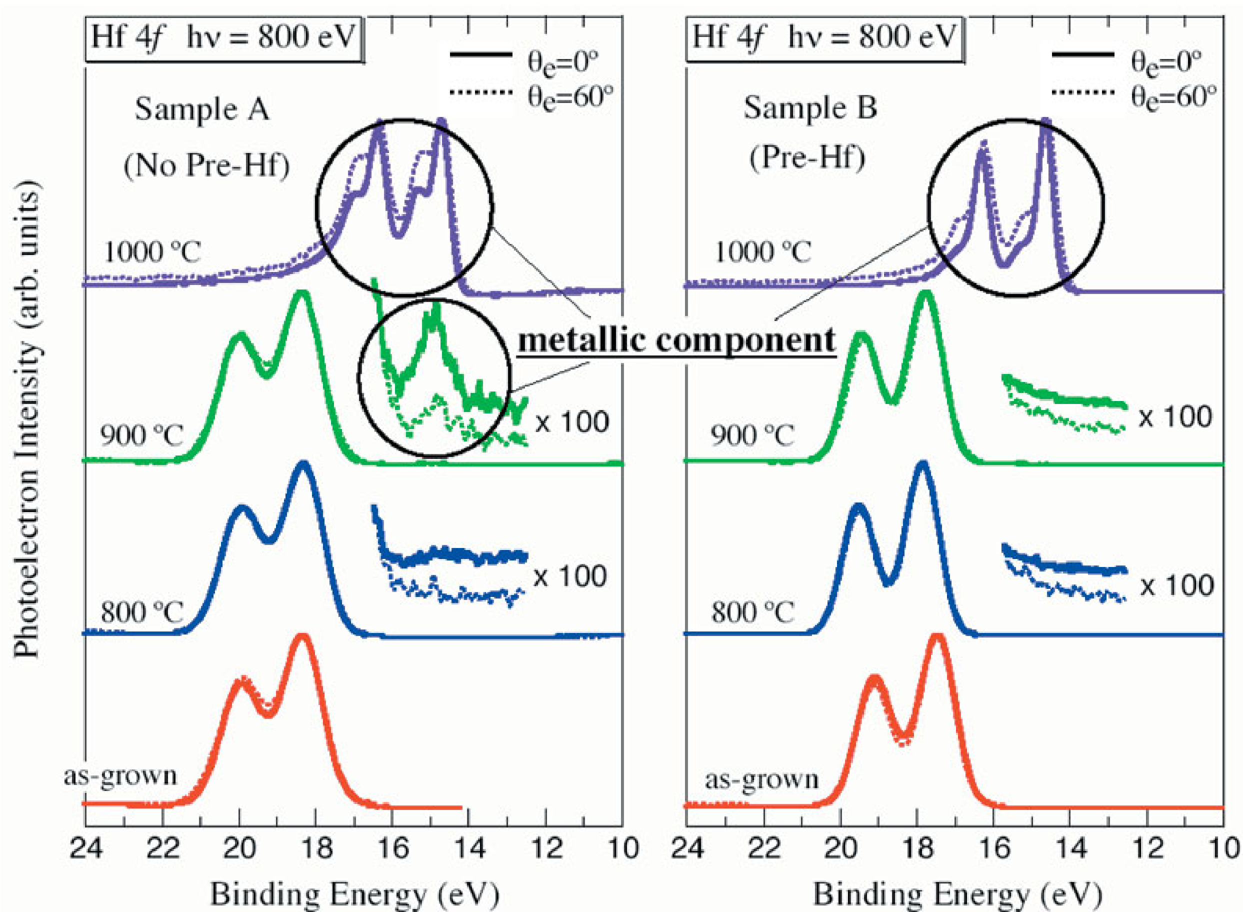

Figure 3

Hf 4*f* photoelectron spectra in HfO_2 without (left panel; Sample A) and with (right panel; sample B) the Hf-metal predeposition with angular dependence of 0°(solid curves) and 60°(dashed curves). Each panel shows the annealing-temperature dependence (as-grown, 800, 900, and 1000°C).

currents. After annealing at 1000°C in ultrahigh vacuum, Hf $4f_{7/2}$ peaks were located at binding energies of 14.6 eV for both films, suggesting that the Hf-O bonding is broken. The Hf-Si and Hf-Hf bondings appear as metallic Hf-silicide and Hf-cluster formations. We also performed *in situ* photoelectron spectroscopy of samples annealed at gradually increasing temperatures spaced by a step of several degrees, and clearly observed the evolution of the HfO_2 reduction processes. Based on these results, more stable gate structures such as SiN interlayers, and Hf-aluminate or Hf-silicate interlayers are being developed in the ULSI fabrication processes.

S. Toyoda, J. Okabayashi and M. Oshima (Univ. of Tokyo)

References

[1] M. Oshima, S. Toyoda, T. Okumura, J. Okabayashi, H. Kumigashira, K. Ono, M. Niwa, K. Usuda and N. Hirashita, *Appl. Phys. Lett.*, **83** (2003) 2172.
[2] S. Toyoda, J. Okabayashi, H. Kumigashira, M. Oshima, K. Ono, M. Niwa, K. Usuda and N. Hirashita, *J. Electron Spectr. Rel. Phenom.*, **137** (2004) 141.
[3] S. Toyoda, J. Okabayashi, H. Kumigashira, M. Oshima, K. Ono, M. Niwa, K. Usuda and G. L. Liu, *Appl. Phys. Lett.*, **84** (2004) 2328.

10-2 Vortex Chirality Control in Mesoscopic Disk Magnets Observed by PEEM

Recent developments in microfabrication techniques allow studies of mesoscopic magnetic structures. Micro- and submicro-meter circular disks have curling in-plane magnetic configurations called vortices. Magnetic vortex structure specific to mesoscopic magnets attract considerable attention due to their importance for ultra-high density data storage technologies such as hard disk drives (HDDs) and magnetic random access memories (MRAMs). The current hot topic is vortex chirality control, the control of clockwise or counter-clockwise magnetic flux circulation in a vortex, however it is quite difficult to realize thermally stable vortex-chirality controllable devices.

Photoelectron emission microscopy (PEEM) has the capability for direct real-space observation of magnetic moments combined with X-ray magnetic circular dichroism (XMCD). Since there is no stray magnetic field from vortices with closed magnetic flux, PEEM is considered as one of the best techniques to observe vortex chirality. The XMCD-PEEM experiments were performed at the undulator beamline NE1B of PF-AR. The PEEM images were acquired at plus and minus helicity circularly polarized photons at the Ni L_3-edge. The magnetic image was then obtained from the difference between the images from plus and minus helicities. The spatial resolution of the PEEM images was estimated to be less than 130 nm. We have designed a chirality-controllable mesoscopic device [Fig. 4(a)] based on a micromagnetic simulation. It is shown that the vortex chirality is determined by the position where the vortex nucleation occurs in the magnetization reversal process. Chirality-controllable mesoscopic devices with tags attached to both side have been designed. The thermal stability of the chirality-controllable devices was also calculated and it was found that the barrier energy is related to the scale of the tags.

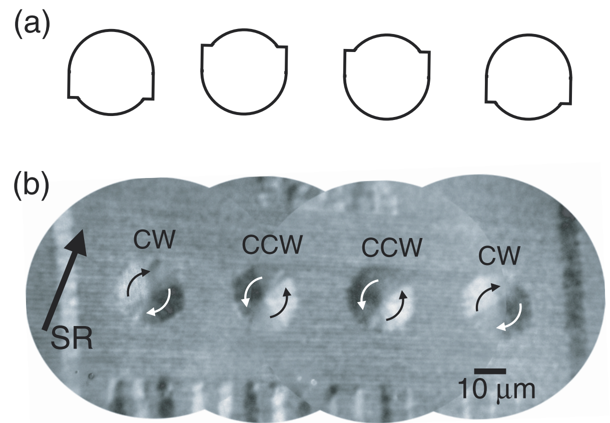

Figure 4
Control of a vortex chirality. (a) Devices for chirality control and (b) PEEM image taken at Ni L_3-edge.

Micrometer-sized vortex-chirality-control device magnets of permalloy were fabricated by electron beam lithography and liftoff techniques. The mesoscopic magnets were also prepared by electron lithography and liftoff techniques. A magnetic field was applied in the atmosphere before the measurement.

The device is a circular disk with tags at each side. The geometry of the devices is shown in Fig. 4(a). Four devices were arranged in alternating directions, the middle two devices have tags on their upper sides, while the disks at either end have tags on their lower sides. In these devices, a vortex always nucleates at the position of the tag during the magnetization reversal process. The chirality of the vortex is determined by the nucleation position of the vortex. Thus the vortex chirality can be controlled by an external magnetic field, that is, either left or right tag.

In order to validate our devices, we have fabricated the vortex-chirality-controlled devices and observed their magnetization distribution by XMCD-PEEM. The external magnetic field was applied to the sample in the atmosphere before the measurement to control the vortex chirality. The magnetic images were taken at the remanence at room temperature. Fig. 4(b) suggests that we have successfully demonstrated the vortex chirality control, that is, the devices with tags on the lower side have a clockwise vortex (the devices at either end), and those with tags on the upper side have a counterclockwise vortex (the middle two disks). This result agrees well with the micromagnetic simulation results. The PEEM images shown in Fig. 4(b) clearly indicate that the vortex chirality

is successfully controlled by the external magnetic fields.

T. Taniuchi[1], M. Oshima[1], H. Akinaga[2] and K. Ono[3]([1]Univ. of Tokyo, [2]AIST, [3]KEK-PF)

10-3 Molecular Mechanism for Regulation of Water Content in Mammalian Skin

In the human body, water accounts for about 60% of total body weight. A huge amount of water is maintained in the human body so as not to be lost through the skin surface. The molecular mechanism for regulation of water content is one of the important problems in skin research. The outermost layer of skin, the stratum corneum (SC), is composed of keratinized cells called corneocytes and intercellular lipids. The flattened corneocytes are embedded in the intercellular lipid matrix. This has been analogized as a brick wall, resulting the “bricks and mortar model”. The mortar, the intercellular lipid matrix, forms a continuous route of molecules from the upper to rear surface in SC and vice versa. The intercellular lipid matrix works not only as the main barrier but also as a pathway for water, drugs, etc. A molecular structural study of the intercellular lipid assembly is highly desired to solve their molecular mechanism. We have proposed a possible mechanism for regulation of water content in a skin based upon the results of a small angle X-ray diffraction experiment performed at BL-15A. We believe that it offers a molecular fundamental basis for the development of not only skin care cosmetics but also for percutaneous drug penetration.

The SC was separated from the skin of a hairless mouse, hydrated with a water content from 0 to 80wt% and subjected to experiments. The multilamellar structures in SC are classified mainly into long lamellar structure (LLS) with about 13 nm [Fig. 5(a)] and short lamellar structure (SLS) with about 6 nm [Fig. 5(b)]. In Fig. 6, X-ray diffraction profiles in hairless mouse SC are shown as a function of water content [1]. With increasing water content, the diffraction peak positions for 1st to 5th order diffraction of LLS are almost unchanged, consistent with the finding of a previous study [2]. On the other hand, the positions of the 1st and 2nd order diffractions of SLS markedly shift towards lower angle, suggesting that SLS exhibits swelling with the increase of the water content. Furthermore, we found that the widths of the diffraction peaks of both LLS and SLS become narrow simultaneously at a water content of 20-30wt% as shown in Fig. 6. Previously it has been known that only the diffraction profile of LLS becomes sharp at the water content of about 20wt% [2]. The present results indicate that LLS and SLS interact with each other, swelling of SLS takes place, and as a result at the water content of 20-30wt% the both LLS and SLS are stabilized simultaneously. It should be pointed out that in SC almost all water is stored in the corneocytes, the so-called bricks, but a small part of water comes out to the water layer of SLS. Once the thickness of the water layer deviates from the steady-state water thickness, owing to the interaction between LLS and SLS, a regulation mechanism works so as to bring back to the steady-state thickness.

Until now the role of SLS has been not noticed yet since the diffraction peak of SLS is sometimes hard to detect. As far as the function of skin associated with hydrophilic nature is considered, we cannot ignore it. In further studies the detailed mechanism of the interaction between LLS and SLS should be clarified.

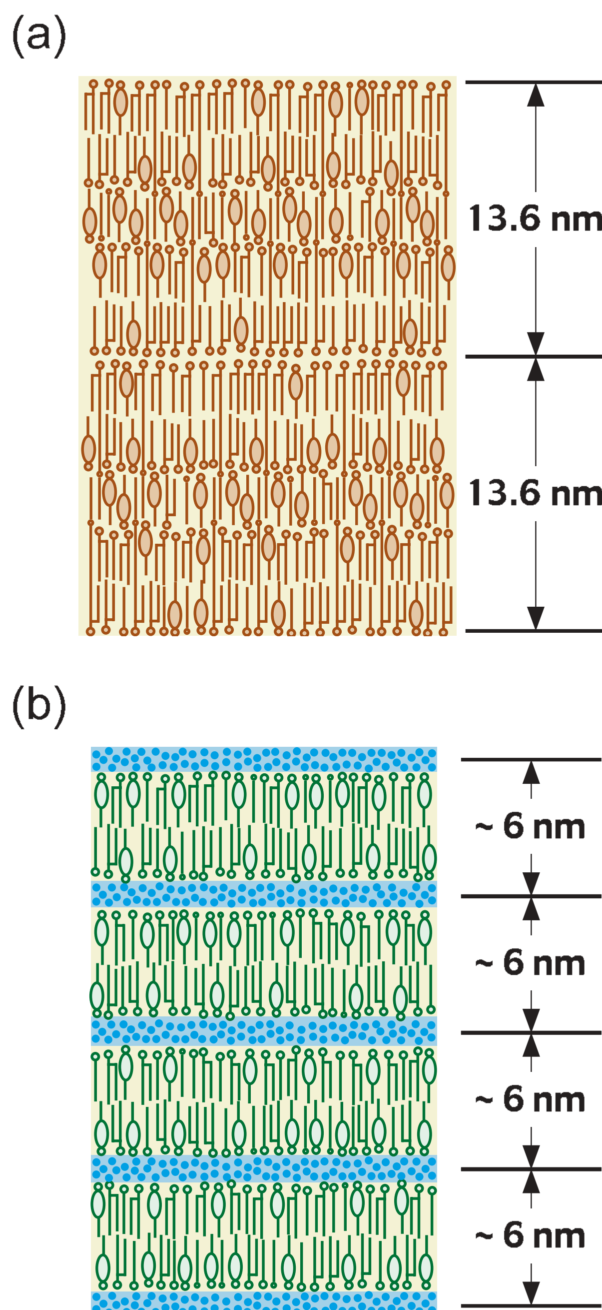

Figure 5
Lamellar structure in the intercellular lipid assembly of stratum corneum where ceramides, fatty acids and cholesterol are drawn schematically. (a) Long lamellar structure (LLS) and (b) short lamellar structure (SLS) in which the water layer is drawn by blue color.

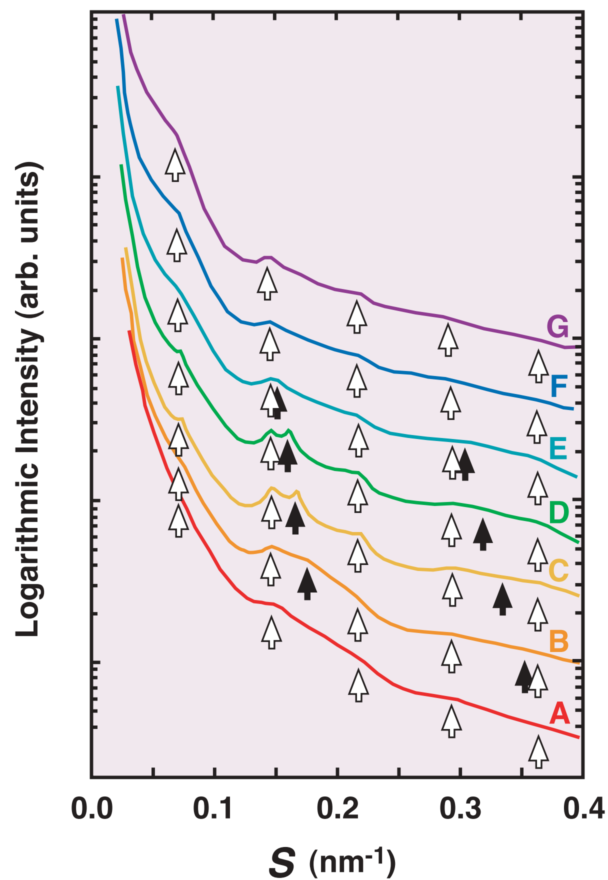

Figure 6
X-ray diffraction intensity for the SC of hairless mouse at the water contents of 0wt% (A), 12wt% (B), 21wt% (C), 35wt% (D), 50wt% (E), 70wt% (F) and 80wt% (G). Open arrows indicate the 1st to 5th order diffraction peaks for LLS and closed arrows indicate the 1st and 2nd order diffraction peaks for SLS.

I. Hatta[1] and N. Ohta[2] ([1]Fukui Univ. of Tech., [2]JASRI)

References

[1] N. Ohta, S. Ban, H. Tanaka, S. Nakata and I. Hatta, *Chem. Phys. Lipids,* **123** (2003) 1.

[2] J.A. Bouwstra, G.S. Gooris, J.A. van der Spek and W. Bras, *J. Invest. Dermatol.*, **97** (1991) 1005.